Supplementary Information

Femtosecond optical orientation triggering magnetization precession in epitaxial EuO films

Vladimir N. Kats,[a] Leonid A. Shelukhin,[a] Pavel A. Usachev,[a] Dmitry V. Averyanov,[b] Igor A. Karateev,[b] Oleg E. Parfenov,[b] Alexander N. Taldenkov,[b] Andrey M. Tokmachev,[b] Vyacheslav G. Storchak [b] and Victor V. Pavlov [a]

[a] Ioffe Institute, 194021 St. Petersburg, Russia

[b] National Research Center "Kurchatov Institute", Kurchatov Sq. 1, Moscow 123182, Russia

Contents:

Note 1. Optical spin orientation *via* the $4f^7 5d^0 \rightarrow 4f^6 5d^1$ electronic transition

In this note we consider the possible orientation mechanisms in EuO discussed by Afanas'ev *et al.*[1] The energy spectrum of the electron states in europium oxide consists of delocalized and localized states. The former set comprises states in the conduction and valence bands, formed as a result of the strong overlap of s, d, and p shells of the Eu and O atoms. The localized states include the states of electrons in the 4f shells of the europium ions Eu^{2+} ($^8S_{7/2}$). The overlap of the wave functions for the 4f shells of neighboring ions is small; as a consequence, the bound-electron approximation is sufficiently accurate to describe the state. The exchange interaction leads to ordering of the spins of the 4f electrons – as soon as temperature drops below 70 K, EuO becomes a ferromagnet. The edge of the optical absorption band of europium oxide comes from transition of electrons from the 4f shells to the conduction band, *i.e.*, $4f^7(^8S_{7/2}) \rightarrow 4f^6(^7F_J)5d^1(t_{2g})$.[2] Analysis of the selection rules for this process[3] has shown that the probability of the optical transition depends on the polarization of the absorbed light and the orientation of the electron spin in the initial and final states. In particular, the most probable transitions under illumination by circularly polarized light are those from levels with the component of the resultant angular momentum (J = 7/2) in the direction of propagation of the incident radiation being of opposite direction to the momentum of the photon. The depletion of these levels should lead to a partial orientation in the spin system of the 4f shells of the Eu^{2+} ions. At the same time, there should be a partial orientation of the electron spins released into the conduction band. The stationary values of the spin orientation of 4f shells and band electrons are determined by the ratio of pumping and relaxation rates. According to the paper by Afanas'ev *et al.*,[1] one can expect a small change in the Curie temperature arising from the indirect exchange interaction. This change is not particularly important to our study of ultrafast dynamics in EuO.

In order to construct a scheme of energy levels in EuO, a number of interactions and their relative strength should be taken into consideration: (i) crystal field splitting of the 5d final state by the Coulomb potential of the crystal lattice; (ii) exchange splitting stemming from the direct spin–spin interaction between electrons in different electronic states; (iii) spin–orbit splitting; (iv) the Zeeman effect in a local magnetic field. The hierarchy of these interactions is demonstrated in Fig. S4.[4-6] The crystal field splits the 5d states into two subbands, a t_{2g}-subband at a lower energy and an e_g-subband at a higher energy; the splitting energy, 3.7 eV, is the largest among the (i)-(iv) interactions.[4] The optical excitation results in a 5d electron and a $4f^6$ state. The excited electron has the spin S_{5d} = 1/2 whereas the six remaining 4f electrons have the spin S_{4f} = 3 according to Hund's rules. The total spin $S_T = S_{4f} \pm S_{5d}$, which amounts to S_T = 5/2 for the antiparallel coupling and S_T = 7/2 for the parallel coupling between the $5d^1$ and the $4f^6$ spins due to the d-f exchange interaction; S_T = 7/2 being energetically more favorable. The 4f electrons are left in a state with the angular moment L_{4f} = 3. In the theoretical model developed by Kasuya,[6] the total spin S_T is coupled to the orbital moment L_{4f} of the 4f electrons to produce the total angular momentum $J = S_T + L_{4f}$ as a consequence of the spin-orbit coupling. The coupling results in two multiplets:

$$S_T = \frac{5}{2}: \quad J = \frac{1}{2}; \frac{3}{2}; \frac{5}{2}; \frac{7}{2}; \frac{9}{2}; \frac{11}{2}. \qquad (1)$$

$$S_T = \frac{7}{2}: \quad J = \frac{1}{2}; \frac{3}{2}; \frac{5}{2}; \frac{7}{2}; \frac{9}{2}; \frac{11}{2}; \frac{13}{2}. \tag{2}$$

Above the Curie temperature, the external magnetic field determines the local magnetic field whereas below T_C, the spontaneous magnetization also contributes. Each of the J levels is degenerate; the Zeeman effect lifts the degeneracy yielding another multiplet with $2J + 1$ sublevels, $-J \leq m_J \leq J$, for each J level.

The absorption edge in EuO is defined by the dipole-allowed spin-preserving transitions satisfying the selection rules

$$\Delta S_T = 0;\ \Delta L = \pm 1;\ \Delta J = 0, \pm 1;\ \Delta m_J = \pm 1. \tag{3}$$

From the initial $4f^7$ ground state with the $^8S_{7/2}$ configuration, three dipole-allowed transitions are possible, to the levels $S_T = 7/2$, J = 5/2, 7/2, and 9/2. One may expect an additional transition to $S_T = 5/2$, J = 7/2 which is a spin–flip transition, and, hence, rather weak.[5] In Fig. S4, the three dipole-allowed transitions and the spin–flip transition are assigned on the basis of magneto-optical spectroscopy[1] by three solid arrows and a dashed arrow, respectively.

Thus, at the pump photon energy of 2.38 eV, electrons are excited into the $5dt_{2g}$ subband. The band-edge absorption coefficient, at a photon energy $\hbar\omega$, can be written as[7]

$$\alpha^{\pm}(\hbar\omega) = \frac{N\pi e^2\hbar\omega}{2c\epsilon_0\hbar}\sum_{J=0}^{6}\sum_{M_J=-J}^{+J}\sum_{X}\left|\mu^{\pm}(J,M_J,X)\right|^2 \times \delta(E_X + E_J - \hbar\omega), \tag{4}$$

where $N = 4/a^3$ is the volume density of the Eu^{2+} ions, and $a =$ 5.144 Å is the EuO lattice constant. The transition changes the energy of the electronic system by $\Delta E = E_J + E_X$, where E_X is the energy of the electron in the final state X. The electric dipole matrix element, associated with such an electronic transition is given for circularly polarized light by[7]

$$\mu^{\pm}(J,M_J,X) = \left[\sum_{m_1=+3}^{7} FM_L = (M_J - 3)M_S = 3|JM_J\right] \times \sum_{m_1=-3} D^{(3)*}_{-M_J+3,m_1}(\alpha_S,\beta_S,\gamma_S) \times \sum_{m'=-2}^{+2} B(X,m') \sum_{m_2=+2}^{m_2=-2} D^{(2)}_{m'm_2}(\alpha_c,\beta_c,\gamma_c) M^{\pm}_{m_1 m_2}, \tag{5}$$

where $D^{(j)}_{mm'}(\alpha,\beta,\gamma)$ are Wigner rotation matrices (explicit forms of these matrices are given in Ref. [8]); α_S,β_S, and γ_S are the Euler angles that transform the reference frame used to describe the $|4fm\rangle$ state; α_c,β_c, and γ_c are the Euler angles that transform the reference frame

of the crystal structure. The matrices $M^{\pm}_{m_1 m_2} = \langle 4f m_1 | x \pm iy | 5d m_2 \rangle$ ($m_1 = -3, \ldots, +3$ and $m_2 = -2, \ldots, +2$) can be derived using the explicit form[9] of the angular part of the atomic $|4fm\rangle$ and $|5dm\rangle$ wave functions:[7]

$$M^{+}_{m_1 m_2} = i r_{df} \begin{bmatrix} \sqrt{\frac{6}{7}} & 0 & 0 & 0 & 0 \\ 0 & \frac{2}{\sqrt{7}} & 0 & 0 & 0 \\ 0 & 0 & \sqrt{\frac{12}{35}} & 0 & 0 \\ 0 & 0 & 0 & \sqrt{\frac{6}{35}} & 0 \\ 0 & 0 & 0 & 0 & \sqrt{\frac{2}{35}} \\ 0 & 0 & 0 & 0 & 0 \\ 0 & 0 & 0 & 0 & 0 \end{bmatrix}, \tag{6}$$

and

$$M^{-}_{m_1 m_2} = r_{df} \begin{bmatrix} 0 & 0 & 0 & 0 & 0 \\ \sqrt{\frac{2}{35}} & 0 & 0 & 0 & 0 \\ 0 & \sqrt{\frac{6}{35}} & 0 & 0 & 0 \\ 0 & 0 & \sqrt{\frac{12}{35}} & 0 & 0 \\ 0 & 0 & 0 & \frac{2}{\sqrt{7}} & 0 \\ 0 & 0 & 0 & 0 & \sqrt{\frac{6}{7}} \end{bmatrix}, \tag{7}$$

where $r_{df} = \int R_{4f}(r) R_{5d}(r) r^3 dr$ is the $4f - 5d$ radial integral. Thus, this analysis demonstrates the presence of electric dipole matrix elements that are nonzero for circularly-polarized light at the $4f^7 5d^0 \rightarrow 4f^6 5d^1$ electronic transition in EuO.

In ferromagnetic EuO, the spins of the 4f shells of neighboring Eu^{2+} ions are practically parallel so that, on the microscopic scale, the spin orientation is nearly complete. When the wave vector of the pump **k** is transverse to the external magnetic field **B** (see Fig. S3), the right (*rcp*) and left circularly polarized (*lcp*) light can equally populate the states of the $5dt_{2g}$ subband with the opposite orientations of the d-electron spin for *rcp* and *lcp*. The magnetization of the 4f shells and band electrons is determined by the generation rate of electron-hole pairs, discussed in Note 2. In the case of linearly polarized light, employing the same geometry, photo-induced magnetization of 4f shells and band electrons is absent due to mutual compensation (linear polarization can be treated as a sum of *lcp* and *rcp*). Thus, linearly polarized light is not expected to cause a magnetization precession. Fig. S5 shows experimental data for linearly-polarized pump pulses: those pulses do not cause magnetization precession. The very small residual signal can arise due to other mechanisms, like laser-induced changes in magnetic anisotropy[10] or the inverse Cotton-Mouton effect.[11]

These mechanisms for circularly-polarized pump light can give rise to a small difference in magnitude of magnetization precession for opposite light helicities.

Note 2. Two mechanisms to trigger magnetization precession in EuO films

In this note, we evaluate two potential mechanisms triggering magnetization precession in EuO films, the optical orientation effect (OOE) and the inverse Faraday effect (IFE), by making numerical estimates for the amplitude of oscillations in the normalized photo-induced magnetization M_z/M_s.

First, we consider the magnetization arising from the OOE, *i.e.* one-photon absorption of the incident circularly polarized light orienting electron spins via a linear optical process:

$$P(\omega) = \epsilon_0 \boldsymbol{\chi} : E(\omega), \tag{8}$$

where $P(\omega)$ is the electric polarization induced in a medium by a light wave with the electric field $E(\omega)$, $\boldsymbol{\chi}$ is the optical susceptibility tensor of the second order. The absorption of photons in a semiconductor follows the Lambert's law:

$$\Phi(x) = \Phi_0 e^{-\alpha x}, \tag{9}$$

where $\Phi(x)$ is the non-absorbed part of photons at a depth x from the surface of the semiconductor, α is the absorption coefficient. The number of incident photons Φ_0 at the front surface can be calculated as:

$$\Phi_0 = \frac{c\epsilon_0 E^2}{n\hbar\omega}, \tag{10}$$

where n is the refractive index of EuO, $\hbar\omega$ is the photon energy of absorbed light and E is the magnitude of the electric field E of the electromagnetic wave.

The generation rate of electron-hole pairs is related to the decrease of the photon flux as:[12]

$$F(x) = -\frac{d\Phi(x)}{dx} = \Phi_0 \alpha e^{-\alpha x} \tag{11}$$

We replace the generation rate by its average value in the film with a thickness l:

$$F_l = \frac{1}{l}\int_0^l \Phi_0 \alpha e^{-\alpha x} dx = \frac{\Phi_0}{l}\left(1 - e^{-\alpha l}\right). \tag{12}$$

The amount of electron-hole pairs is a product of the generation rate F_l and the pulse time duration t_p. As a result of the optical orientation, the spins of the photo-induced electrons are directed along the pump wave vector; each electron produces an effective magnetic moment $g\sqrt{J(J+1)}\mu_B$, where J is the total angular momentum, g is the g-factor of the $5d^1$-electron, and μ_B is the Bohr magneton. Based on Eq. (10) and Eq. (12), we can express the photo-induced magnetization of the OOE as

$$M^{OOE} = \frac{c\epsilon_0 g\sqrt{J(J+1)}\mu_B t_p}{nl\hbar\omega}\left(1 - e^{-\alpha l}\right)E^2 . \tag{13}$$

In order to estimate the photo-induced magnetization, we express E^2 for circularly polarized light in terms of measurable quantities:

$$E^2 = \frac{nJ_p}{c\epsilon_0 t_p}, \tag{14}$$

where J_p is the pulse fluence. To estimate the OOE magnetization, we use the following parameters – the EuO film thickness $l =$ 97 nm, the refractive index $n = Re\sqrt{\epsilon_1 + i\epsilon_2} =$ 1.6 (ϵ_1 and ϵ_2 being the real and imaginary parts of the optical dielectric function provided by Ref. [13]), $\alpha = 2\pi\epsilon_2/n\lambda$, $1 - e^{-\alpha l} =$ 0.56.

The photo-induced magnetization M^{OOE} affects the magnetic moment of the f-electron system through a strong exchange interaction between the excited 5d-electrons and 4f-electrons of Eu^{2+} ions. In other words, a magnetic field $H^{OOE} \sim M^{OOE}$ acts on 4f-electrons during the spin lifetime τ_s of excited 5d-electrons (in other chalcogenides EuX (X = Te, Se), pump-probe measurements estimate τ_s of the order of several tens of picosecond[14,15]).

To analyse the IFE, we consider the corresponding magnetic field H^{IFE}. Phenomenologically, $H^{IFE}(0)$ can be parametrically generated by a light wave with frequency ω through a two-photon process.[16] The laser-induced magnetic field H^{IFE} is non-zero during the pulse time only[17-19] (for the International System of Units notation, see Ref. [20]):

$$H^{IFE}(0) = -i\frac{\epsilon_0 G}{\mu_0 M_s} Im\{E(\omega) \times E^*(\omega)\} , \tag{15}$$

where G is the medium gyration responsible for the magneto-optical Faraday rotation, which can be calculated from the published data on the magneto-optical Kerr effect in EuO (the complex polar Kerr effect $\theta_K + i\epsilon_K \simeq (-3 + i)\pi/180$ rad for $\hbar\omega =$ 2.38 eV and $T =$ 10 K[4,21]) and the complex optical dielectric function.[13]

The subpicosecond laser pumping used in the experiment corresponds to an envelope of electromagnetic waves with the Gaussian profile:

$$I(t) \propto \frac{1}{\sigma\sqrt{2\pi}} exp(-\frac{t^2}{2\sigma^2}), \tag{16}$$

where $\sigma = t_p/\sqrt{ln256}$ is the *rms* width of the laser pulse. It is important that the laser-induced magnetic field H^{IFE} must vanish outside the laser pulse interval when $-t_p < t < t_p$ in the process described by Eq. (15). Next, we consider the process of magnetization precession triggering for the pulse laser pumping in more detail.

In the case of the subpicosecond laser pulse, the field H^{IFE} should be determined mainly by the diamagnetic contribution to the IFE[22] because in our experiment the magnetization initially lies in the plane of the sample and cannot respond quickly to the external ultrafast impact.[23] Thus, an estimate of the IFE based on the medium gyration G would be an upper bound because it includes both the diamagnetic- and magnetization-dependent contributions. H^{IFE} is parallel to the electromagnetic wave vector k which sign depends on the chirality of the wave $\sigma^{\pm}$. The magnetic moment of the 4f-shell lying in the sample plane starts to precess with the frequency Ω. The precession takes place around an effective magnetic field H^{*}_{eff}, which is the vector sum of H_{eff} and the laser-induced magnetic field H^{IFE}. Fig. 5d demonstrates the geometry for triggering the magnetization precession. Due to the anisotropy, described in the main text, the magnetization precession has a complicated shape, an ellipse sticking to a spherical surface. However, in the experiment, we do not see this anisotropy because only the z-component of magnetization is detected. In that case, one can use the uniaxial magnetic anisotropy for simulation which simplifies the analysis significantly. The amplitude of the z-component of the magnetization can be written as:

$$M_z^{IFE} = M_s \, sin\varphi \, cos\varphi, \tag{17}$$

where $\varphi = arctan\left(H^{IFE}/H_{eff}\right)$. Upon the termination of the laser pulse, the precession of magnetization continues around the former direction of H_{eff}.

Upon action of H^{OOE} or H^{IFE} the magnetic moment of the 4f-electrons starts to precess in accordance with the Landau-Lifshitz–Gilbert equation:[24]

$$\frac{dM}{dt} = -\gamma M \times H_{eff} + \alpha M \times \frac{dM}{dt}, \tag{18}$$

where M is the magnetization, γ is the electron gyromagnetic ratio, α is the Gilbert damping parameter, and H_{eff} is the effective magnetic field:

$$H_{eff} = H_0 + H_{anis} + H_{dem}, \tag{19}$$

where H_0 is the external magnetic field, H_{anis} is the anisotropy field, and H_{dem} is the demagnetization field.

We carried out numerical simulations based on Eq. (18), taking into account the experimental geometry (Fig. 5d) and the temporal changes of magnetic fields induced by the electromagnetic wave with the Gaussian profile (see Eq. (16)) due to the IFE and the OOE. Time dependence of H^{OOE} can be modelled as:[25,26]

$$H^{OOE}(t) \propto exp\left(\frac{\sigma^2}{\tau_s^2} - \frac{t}{\tau_s}\right)\left[1 - erf\left(\frac{\sigma}{\tau_s} - \frac{t}{2\sigma}\right)\right], \tag{20}$$

where τ_s is the spin lifetime of the $5d^1$ electron state. This function describes the temporal evolution of the Weiss magnetic field $H^{OOE} = \frac{\lambda M^{OOE}}{\mu_0}$ which influences the magnetic moment of the f-electron system *via* the strong exchange interaction between the excited 5d-electrons and 4f-electrons of Eu^{2+} ions with a parameter λ.[27,28] To evaluate M_z^{IFE}, we employ Eq (14) taking into account the decay of light intensity inside the EuO film $(1 + e^{-\alpha l})/2 = 0.72$ and Eq. (15). Upon normalizing, we obtain $M_z^{IFE}/M_s = 1.2 \cdot 10^{-4}$ for the magnetic field of 200 mT. This value is too low to describe the experimental data on EuO. In contrast, the value of $M_z^{OOE}/M_s = 4.6 \cdot 10^{-3}$, calculated according to Eq. (13) and (14), is large enough to describe the experimental data. The results of simulations for the temporal evolution of photo-induced magnetization are presented in Fig. S6. In particular, Fig. S6a and S6b show temporal changes of the magnetic field H^{OOE} and the photo-induced magnetization M_z^{OOE} excited via OOE. Fig. S6c and S6d demonstrate the same characteristics for the IFE. The calculations show a strong difference in the magnitudes of M_z^{OOE} and M_z^{IFE}. A key result is the difference in the initial phases. M_z^{OOE}/M_s exhibits a cosine-like initial phase in agreement with the experiment. In contrast, M_z^{IFE}/M_s demonstrates a sine-like initial phase. This result agrees with an elaborate quantum mechanical approach to the IFE[29]; a sine-like phase, however, does not correspond to our observations. Thus, the simulations support the OOE as a plausible mechanism for triggering the magnetization precession in epitaxial EuO films.

Finally, it would be informative to evaluate the decay time τ_o of the oscillations and the spin lifetime τ_s of photo-excited d-electrons from the experimental data. To this purpose, we employ the following fitting function:

$$M_z/M_s = Ae^{-t/\tau_0}\cos \Omega t + Be^{-t/\tau_s} + C, \tag{21}$$

i.e. a combination of an oscillating contribution, a temporal variation of photo-induced magnetization due to the MOKE, and a magnetization due to the quadratic Kerr effect.[30] Fits of the pump-probe data at 200 mT (Fig. S2) provide the following estimates: in EuO, the decay time $\tau_o =$ 663(42) ps and the spin lifetime $\tau_s =$ 114(9) ps; in Eu(Gd)O, $\tau_o =$

269(44) ps and $\tau_s =$ 88(16) ps. Eu(Gd)O has a significantly higher carriers concentration; therefore, scattering of photo-excited electron spins results in shorter spin lifetime τ_s and decay time of the oscillations τ_o. It also explains smaller values of the fitting coefficients A, B and C in Eu(Gd)O. A strong difference between the spin lifetime τ_s and the laser pulse time t_p $(\tau_s \gg t_p)$ is one of the main reasons for the dominance of the OOE over the IFE in triggering the magnetization precession in epitaxial EuO films.

References

1 M. M. Afanas'ev, M. E. Kompan, I. A. Merkulov, *Sov. Phys. JETP*, 1976, **44**, 1086.
2 G. Busch, P. Wachter, *Z. Angew. Phys.,* 1968, **26**, 1.
3 J. O. Dimmock, J. Hanus, J. Feinleib, *J. Appl. Phys.*, 1970, **41**, 1088.
4 J. Schoenes, *J. Magn. Soc. Jpn.*, 1987, **11** (Suppl. S1), 99.
5 P. Fumagalli, J. Schoenes, *Magneto-Optics: An Introduction*. De Gruyter: Berlin, Boston, 2021.
6 T. Kasuya, *CRC Critical Reviews in Solid State Sciences*, 1972, **3**, 131.
7 A. B. Henriques, M. A. Manfrini, P. H. O. Rappl, E. Abramof, *Phys. Rev. B*, 2008, **77**, 035204.
8 D. A. Varshalovich, A. N. Moskalev, V. K. Khersonskii, *Quantum Theory of Angular Momentum* (World Scientific, Singapore, 1988).
9 L. D. Landau, E. M. Lifshitz, *Quantum Mechanics. Non-relativistic Theory* (Pergamon Press, Oxford, 1991).
10 L. A. Shelukhin, V. V. Pavlov, P. A. Usachev, P. Yu. Shamray, R. V. Pisarev, A. M. Kalashnikova, *Phys. Rev. B*, 2018, **97**, 014422.
11 A. M. Kalashnikova, A. V. Kimel, R. V. Pisarev, V. N. Gridnev, A. Kirilyuk, Th. Rasing, *Phys. Rev. Lett.*, 2007, **99**, 167205.
12 R. Alcubilla, C. Voz, *Selected Problems in Semiconductor Physics and Electronic Devices*. Universitat Politécnica de Catalunya: Barcelona, 2020.
13 G. Güntherodt, *Phys. Condens. Matter*, 1974, **18**, 37.
14 V. V. Pavlov, R. V. Pisarev, S. G. Nefedov, I. A. Akimov, D. R. Yakovlev, M. Bayer, A. B. Henriques, P. H. O. Rappl, E. Abramof, *J. Appl. Phys.*, 2018, **123**, 193102.
15 A. B. Henriques, X. Gratens, P. A. Usachev, V. A. Chitta, G. Springholz, *Phys. Rev. Lett.*, 2018, **120**, 217203.
16 Y. R. Shen, *The Principles of Nonlinear Optics*. Wiley-Interscience: New York, 1984.
17 L. P. Pitaevskii, *Sov. Phys. JETP*, 1961, **12**, 1008.
18 J. P. van der Ziel, P. S. Pershan, L. D. Malmstrom, *Phys. Rev. Lett.*, 1965, **15**, 190.
19 P. S. Pershan, J. P. van der Ziel, L. D. Malmstrom, *Phys. Rev.*, 1966, **143**, 574.
20 M. A. Kozhaev, A. I. Chernov, D. A. Sylgacheva, A. N. Shaposhnikov, A. R. Prokopov, V. N. Berzhansky, A. K. Zvezdin, V. I. Belotelov, *Sci. Rep.*, 2018, **8**, 11435.
21 A. K. Zvezdin, V. A. Kotov, *Modern Magnetooptics and Magnetooptical Materials*. CRC Press: Boca Raton, 1997.
22 A. H. M. Reid, A. V. Kimel, A. Kirilyuk, J. F. Gregg, Th. Rasing, *Phys. Rev. B*, 2010, **81**, 104404.

23 D. Popova, A. Bringer, S. Blügel, *Phys. Rev. B*, 2011, **84**, 214421.
24 R. Mondal, M. Berritta, P. M. Oppeneer, *Phys. Rev. B*, 2016, **94**, 144419.
25 A. V. Kimel, F. Bentivegna, V. N. Gridnev, V. V. Pavlov, R. V. Pisarev, Th. Rasing, *Phys. Rev. B*, 2001, **63**, 235201.
26 D. J. Hilton, C. L. Tang, *Phys. Rev. Lett.*, 2002, **89**, 146601.
27 S. Blundell, *Magnetism in Condensed Matter*. Oxford University Press: Oxford, 2001.
28 S. C. P. van Kooten, X. Gratens, A. B. Henriques, *Phys. Rev. B*, 2021, **103**, 035202.
29 D. Popova-Gorelova, A. Bringer, S. Blügel, *Phys. Rev. B*, 2021, **104**, 224418.
30 V. N. Kats, S. G. Nefedov, L. A. Shelukhin, P. A. Usachev, D. V. Averyanov, I. A. Karateev, O. E. Parfenov, A. N. Taldenkov, A. M. Tokmachev, V. G. Storchak, V. V. Pavlov, Appl. Mater. Today, 2020, 19, 100640.

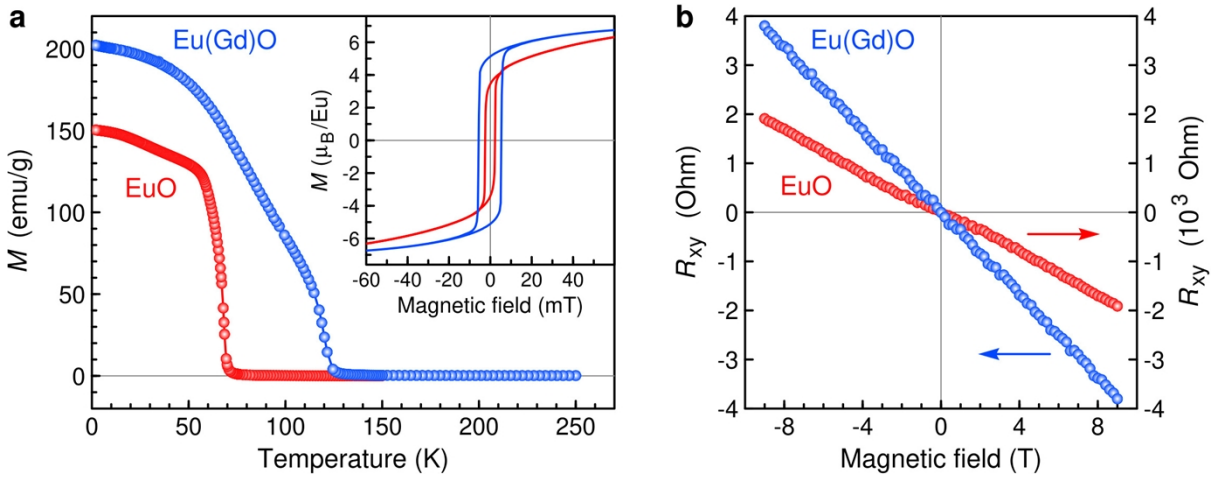

Figure S1. Magnetic and transport properties of EuO-based films – pristine EuO (red) and Eu(Gd)O (blue). (a) Temperature dependence of magnetization in an in-plane magnetic field of 10 mT; inset demonstrates magnetic field dependence of magnetic moment per Eu atom at 2 K. (b) Magnetic field dependence of the Hall conductivity at 20 K.

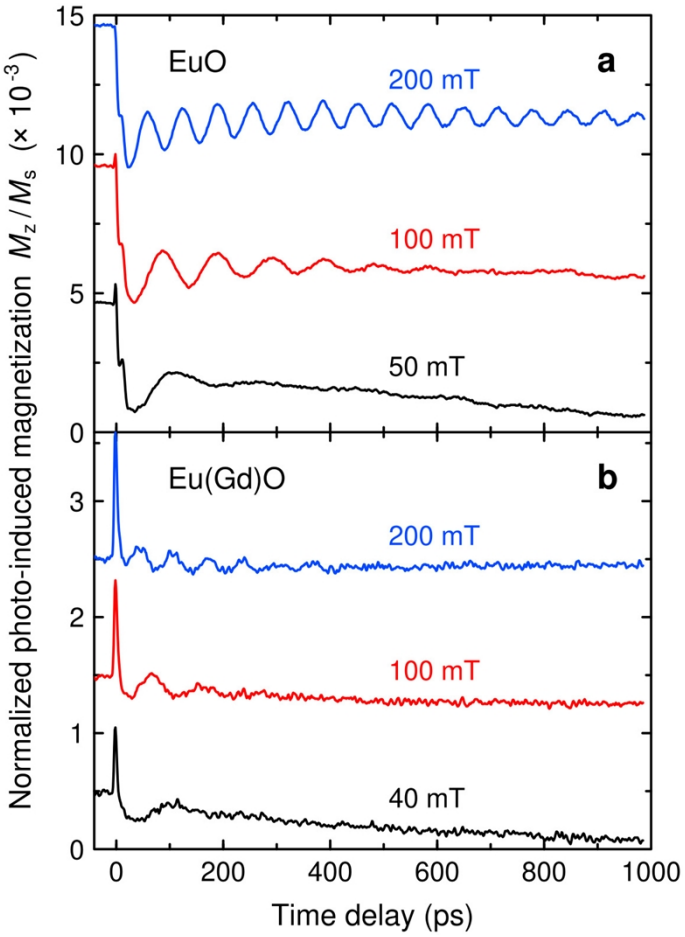

Figure S2. Dynamics of magnetization excited by femtosecond laser pulses. (a) Normalized photo-induced magnetization of EuO at 20 K in magnetic fields 50 mT (black), 100 mT (red), and 200 mT (blue). (b) Normalized photo-induced magnetization of Eu(Gd)O at 20 K in magnetic fields 40 mT (black), 100 mT (red), and 200 mT (blue).

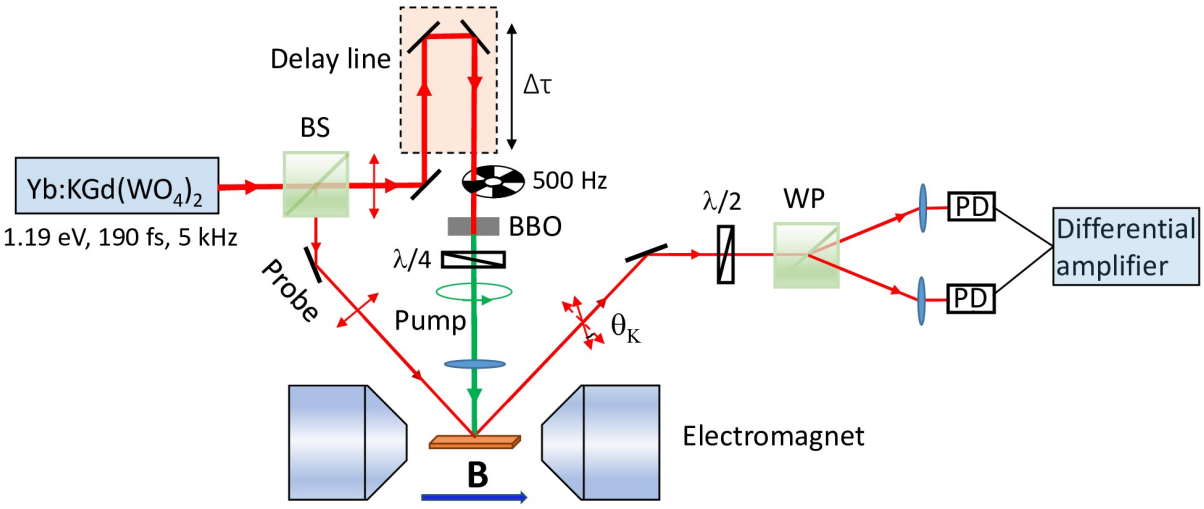

Figure S3. An optical scheme of the experimental setup based on the two-colour pump-probe technique. BS – a beam splitter, BBO – a nonlinear crystal of beta barium borate, $\lambda/4$ – a quarter-wave plate, $\lambda/2$ – a half-wave plate, WP – a Wollaston prism, PD – a photodiode. The wave vector of the pump beam is parallel to the sample normal, the angle between the wave vector of the probe beam and the sample normal is about 10°.

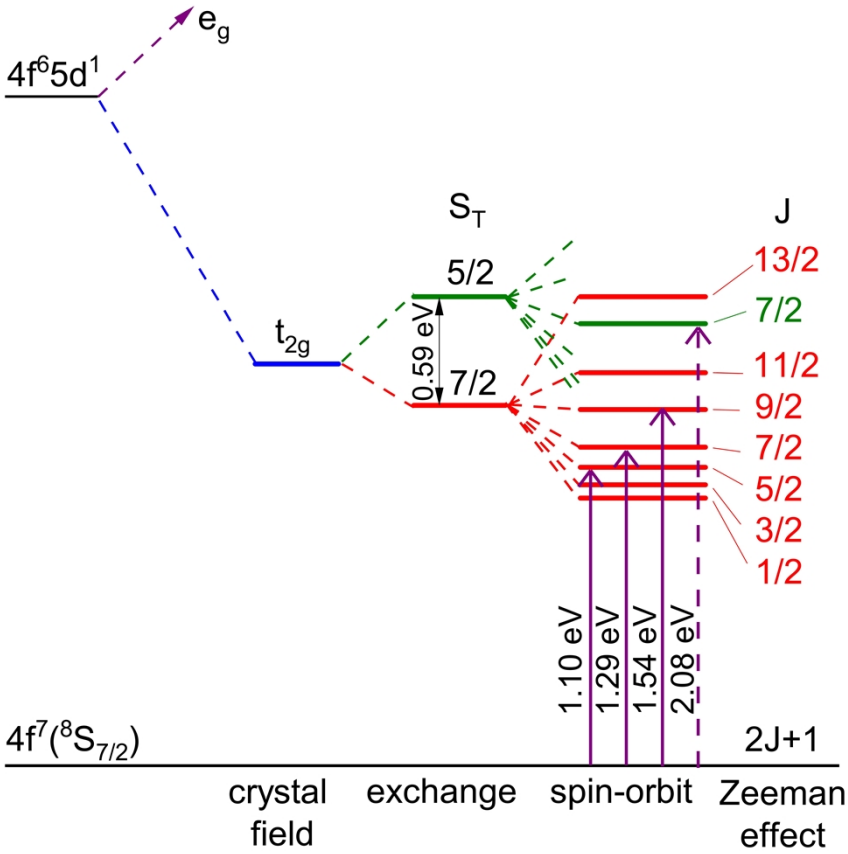

Figure S4. Energy-coupling scheme for the $4f^75d^0 \rightarrow 4f^65d^1$ electronic transition responsible for the formation of the absorption edge in EuO.[4-6]

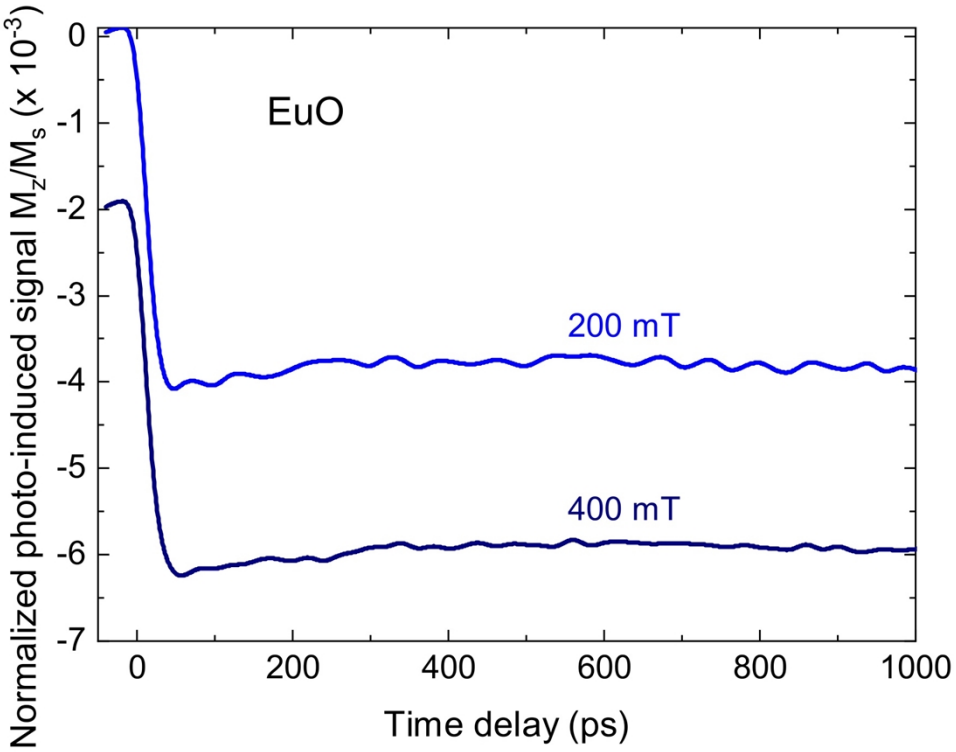

Figure S5. Dynamics of magnetization excited by linearly polarized pump pulses in EuO at 20 K in magnetic fields 200 mT and 400 mT.

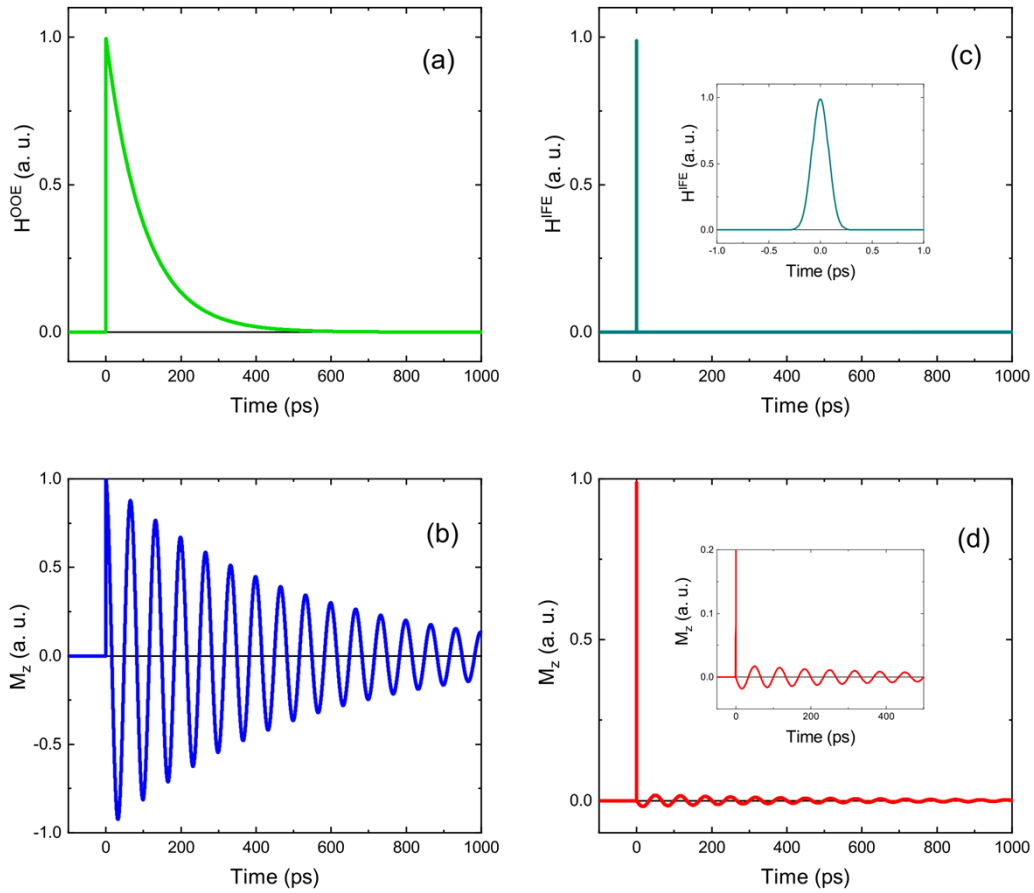

Figure S6. Results of calculations based on solving Eq. (18) for the temporal evolution of the stimulating magnetic field and the magnetization precession. Time dependence of (a) the magnetic field H^{OOE}; (b) the photo-induced magnetization M_z^{OOE}; (c) the magnetic field H^{IFE}; (d) the photo-induced magnetization M_z^{IFE}. The insets in (c) and (d) show the scaled graphs. The calculations employ the following parameters: a laser pulse time τ_p of 0.19 ps, a spin lifetime τ_s of 100 ps, a decay time τ_o of 500 ps, and a precession period of 67 ps.